JACS
JOURNAL OF THE AMERICAN CHEMICAL SOCIETY
Article
pubs.acs.org/JACS

Dynamic Coupling among Protein Binding, Sliding, and DNA Bending Revealed by Molecular Dynamics

Cheng Tan,[†] Tsuyoshi Terakawa,[‡] and Shoji Takada*[,†]

[†]Department of Biophysics, Graduate School of Science, Kyoto University, Kyoto 606-8502, Japan
[‡]Department of Biochemistry and Molecular Biophysics, Columbia University, New York, New York 10032, United States

Supporting Information

ABSTRACT: Protein binding to DNA changes the DNA's structure, and altered DNA structure can, in turn, modulate the dynamics of protein binding. This mutual dependency is poorly understood. Here we investigated dynamic couplings among protein binding to DNA, protein sliding on DNA, and DNA bending by applying a coarse-grained simulation method to the bacterial architectural protein HU and 14 other DNA-binding proteins. First, we verified our method by showing that the simulated HU exhibits a weak preference for A/T-rich regions of DNA and a much higher affinity for gapped and nicked DNA, consistent with biochemical experiments. The high affinity was attributed to a local DNA bend, but not the specific chemical moiety of the gap/nick. The long-time dynamic analysis revealed that HU sliding is associated with the movement of the local DNA bending site. Deciphering single sliding steps, we found the coupling between HU sliding and DNA bending is akin to neither induced-fit nor population-shift; instead they moved concomitantly. This is reminiscent of a cation transfer on DNA and can be viewed as a protein version of polaron-like sliding. Interestingly, on shorter time scales, HU paused when the DNA was highly bent at the bound position and escaped from pauses once the DNA spontaneously returned to a less bent structure. The HU sliding is largely regulated by DNA bending dynamics. With 14 other proteins, we explored the generality and versatility of the dynamic coupling and found that 6 of the 15 assayed proteins exhibit the polaron-like sliding.

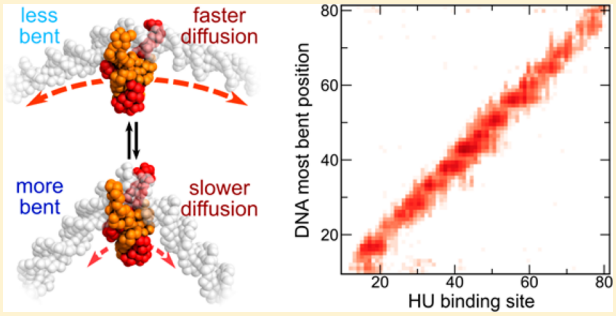

INTRODUCTION

Many DNA-binding proteins interact dynamically with DNA as they search for target sites. Transcription factors search for their recognition element DNA sequences, whereas types of DNA repair machinery look for mismatches or DNA strand breaks. During these search processes, the dominant protein−DNA interactions are nonspecific, and yet there has been less focus on these interactions than on the specific ones directly involved in genetics. Yet nonspecific protein−DNA interactions play crucial roles in many gene regulation and organization processes. For example, one-dimensional diffusion, or sliding, of transcription factors[1−3] and the compaction of DNA by architectural proteins involve such nonspecific interactions.[4,5] Here, we focus on the dynamic aspects of nonspecific protein−DNA interactions.

Protein−DNA interactions markedly change DNA structure,[6−8] and altered DNA structure modulates protein−DNA interactions and protein motions on DNA.[9−13] The underlying molecular mechanisms of the interplay among protein−DNA binding, DNA deformation, and protein sliding is fundamental to our understanding of a wide variety of cellular processes. Experiments have characterized the effect of protein binding on the apparent bend and twist flexibilities of DNA.[6,14−16] Two well-known examples are the eukaryotic nucleosome, in which 147 base pairs (bp) of double-stranded DNA (dsDNA) wrap around the histone core by one and three-fourths turns,[17] and the prokaryotic nucleoid, where architectural DNA-binding proteins are used to pack genomic DNA into living cells.[4,18] In these examples the intrinsic bending preferences of DNA are crucial in determining the binding mechanisms of proteins.[12,19−22] Additionally, very subtle variances in the DNA backbone topography can result in distinguishable binding properties for different proteins belonging to the same family.[12,23] Experimental and theoretical works found that DNA bending also played important roles in the recognition of DNA mismatch by protein MutS.[24−26] These results suggest that the binding of proteins and the conformations of the underlying DNA are mutually responsive.

Most of this knowledge is based on static structural studies. The dynamic aspects of these interactions are much more difficult to address. Single-molecule experiments have provided interesting evidence that some transcription factors and enzymes search DNA using more than one mode of diffusion,[27−29] and even pause occasionally when encountering specific DNA sequences or structures.[30−32] However, these experiments focused on relatively long-time behavior because of limited temporal and spatial resolutions.

Received: April 11, 2016
Published: June 16, 2016

DOI: 10.1021/jacs.6b03729
J. Am. Chem. Soc. 2016, 138, 8512−8522

Here we address the dynamic coupling between protein sliding on DNA and DNA bending by employing a molecular dynamics (MD) simulation approach. Although MD simulations have been widely used to study the detailed dynamics of protein−DNA interactions,[33−40] it is still difficult for atomic MD simulations to simulate a typical sized protein−DNA binding system for time scales long enough to elucidate dynamic coupling. Instead, recent coarse-grained (CG) MD simulation studies of the target search processes of transcription factors have shown promise in investigating protein−DNA binding, sliding, and recognition mechanisms.[33,35,36,41−44] Besides, recent efforts to develop more sophisticated CG models, including the atomic interaction-based coarse-grained (AICG) model for proteins[45] and the latest version of the three-site-per-nucleotide (3SPN.2C) model for DNA,[46] have provided promising tools for accurate modeling of protein and DNA structures, as well as protein−DNA interactions.[47,48] Notably, the 3SPN.2C model of DNA has been carefully designed so that sequence-dependent dsDNA conformations and bending rigidity are accurately represented, enabling us to address the issue of coupling between protein binding and DNA deformation.

To address this issue on an ideal model system, we used the histone-like protein from strain U93 (HU).[49] HU is one of the most abundant DNA-binding proteins in *E. coli*,[4] and is involved in many important cellular processes, such as transcription repression,[50,51] DNA repair[52−54] and most conspicuously, DNA compaction.[55] Despite its varied biological functions, HU has a relatively simple structure. HU is either a homodimer or a heterodimer of two highly homologous subunits, HUα and HUβ, each consisting of around 90 amino acid residues.[56,57] The two positively charged subunits form an α-helical dimerization core and two flexible β-sheet arms[58] (Figure 1). HU wraps around diverse DNA structures with the β-sheet arms binding to the minor grooves as indicated by the crystal structure of HU−DNA complex. We note that in these structures the DNAs have flipped-out bases and mismatches.[59] Normally HU is classified as a sequence-nonspecific DNA-binding protein, but recent studies show that HU has a weak preference for A/T-rich sequences.[60,61] In contrast to the weak sequence preference, biochemical experiments have clearly revealed that HU binds to special DNA structures, such as nicks, gaps, or cruciform junctions, with much higher affinity than to linear DNA.[62,63] Atomic force microscopy experiments also demonstrated that HU binding facilitates the bending of DNA,[64] although there seems to be no specific bending angle.[59,64] Accordingly, the HU binding site size on DNA has been reported to cover a very wide range, from 6 to 34 bp.[59,65,66] Despite the crucial roles HU plays in cellular processes and the available experimental results of HU−DNA binding properties, the detailed mechanism of HU binding, diffusion, and induced DNA bending at the molecular level is still missing.

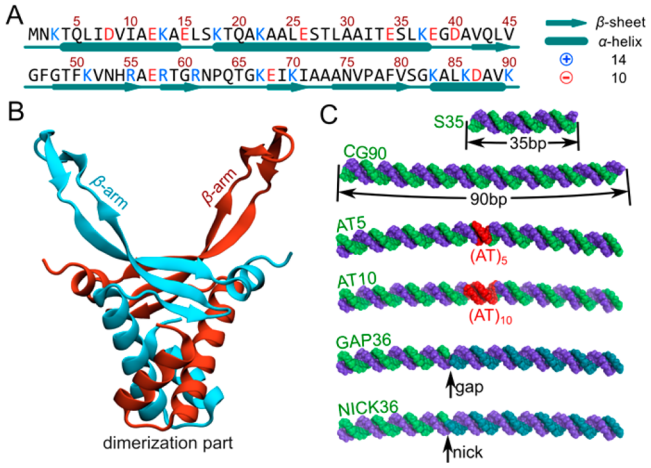

Figure 1. *E. coli* HU α_2 dimer and DNAs used in this study. (A) Sequence and secondary structure features of HU α-subunit. Positively (negatively) charged residues are in blue (red). (B) HU α_2 homodimer with the two chains shown in different colors. (C) The reference structures of DNA molecules studied. The short 35-bp dsDNA (S35) was employed for calibration of the intermolecule interactions. The other 90-bp dsDNAs were used in the production runs to study HU binding. From top to bottom: CG90:90-bp dsDNA of only C/G; AT5 (AT10): five (ten) A/T base pairs at the center; GAP36 (NICK36): having a gap (nick) at DNA index 36. Sequences of these dsDNAs are listed in Table 1.

In this work, we first performed extensive MD simulations of HU binding to DNA with different sequence or structural properties. We confirmed that the sequence-dependent or topology-dependent deviations of DNA conformation affect the preferred binding site of HU, which is consistent with biochemical experimental results.[60−63] Then, we demonstrate that the binding of HU increases the bending angle of DNA, which in turn results in different diffusion modes of HU. Dynamically, the HU sliding is highly coupled with local DNA bending, which is reminiscent of a polaron in physics: an electron or cation self-trapped by the structural deformation of its surrounding medium.[67−69] On shorter time scales, we observed that HU pauses when DNA at the HU binding position is highly curved, and resumes diffusing when DNA spontaneously returns to less bent states. Finally, by exploring 14 other DNA-binding proteins, we address the generality and versatility of the coupling between protein−DNA binding and DNA conformational changes. We find that some, but not all, proteins exhibit polaron-like sliding, as observed for HU.

RESULTS

Modeling HU Binding to DNA and Model Validations.

In the present work, we employed coarse-grained (CG) molecular models where each amino acid in the HU protein is represented by one particle located at its C_α position, while each nucleotide is simplified as three beads, representing phosphate, sugar, and base. For energy functions, we used the AICG2+ model[45] for the HUα_2 homodimer and the 3SPN.2C model[46] for DNA (see Methods section for details). HUα_2 remained a homodimer throughout the study, so hereafter we designate it simply as HU. For protein−DNA interactions, electrostatic and excluded volume effects were included.

To optimize and validate the computational model, we utilized experimental data for binding affinities of HU to various DNA sequences. First, the dissociation constant K_d for a linear 35-bp dsDNA was measured as 9 μM.[62] HU binding to DNA is largely nonspecific, but shows a weak preference for AT-rich sequences in biochemical studies.[60,61] Orders of magnitude smaller K_d's were reported for DNAs with a nick (K_d = 40 nM) and a gap (K_d = 11 nM).[62]

We first calibrated the binding affinity of HU to the 35-bp dsDNA used in the experiment described above[62] by changing the phosphate charge. By simulating reversible HU binding to DNA, we can "measure" K_d in our computational model (see

DOI: 10.1021/jacs.6b03729
J. Am. Chem. Soc. 2016, 138, 8512−8522

Table 1. Sequences of dsDNAs We Used in Simulations

DNA label	sequence
S35	5'-CCCTATAACCCCTGCATTGAATTCCAGTCTGATAA-3' 3'-GGGATATTGGGGACGTAACTTAAGGTCAGACTATT-5'
CG90	5'-GCGGCCCCGGGGCGCGCCCCGGGCGCCGCCGCGCCCGGCGGGGCCGCCGGCCGGGGCCGGCGGGCCGGCGCGGGGGCGCGGCCGCGCCCG-3' 3'-CGCCGGGGCCCCGCGCGGGGCCCGCGGCGGCGCGGGCCGCCCCGGCGGCCGGCCCCGGCCGCCGGCCGCGCCCCGCGCCGGCGCGGGC-5'
AT5	5'-GCGGCCCCGGGGCGCGCCCCGGGCGCCGCCGCGCCCGGCGGGGCCATTTACCGGGGCCGGCGGGCCGGCGCGGGGGCGCGGCCGCGCCCG-3' 3'-CGCCGGGGCCCCGCGCGGGGCCCGCGGCGGCGCGGGCCGCCCCGGTAAATGGCCCCGGCCGCCCGGCCGCGCCCCCGCGCCGGCGCGGGC-5'
AT10	5'-GCGGCCCCGGGGCGCGCCCCGGGCGCCGCCGCGCCCGGCGATATATATAACCGGGGCCGGCGGGCCGGCGCGGGGGCGCGGCCGCGCCCG-3' 3'-CGCCGGGGCCCCGCGCGGGGCCCGCGGCGGCGCGGGCCGCTATATATATTGGCCCCGGCCGCCCGGCCGCGCCCCCGCGCCGGCGCGGGC-5'
GAP36	5'-GCGGCCCCGGGGCGCGCCCCGGGCGCCGCCGCGCC-3' 5'-GGCGGGGCCGCCGGCCGGGGCCGGCGGGCCGGCGCGGGGGCGCGGCCGCGCCCG-3' 3'-CGCCGGGGCCCCGCGCGGGGCCCGCGGCGGCGCGGGCCGCCCCGGCGGCCGGCCCCGGCCGCCGGCCGCGCCCCGCGCCGGCGCGGGC-5'
NICK36	5'-GCGGCCCCGGGGCGCGCCCCGGGCGCCGCCGCGCC-3' 5'-GGCGGGGCCGCCGGCCGGGGCCGGCGGGCCGGCGCGGGGGCGCGGCCGCGCCCG-3' 3'-CGCCGGGGCCCCGCGCGGGGCCCGCGGCGGCGCGGGCCGCCCCGGCGGCCGGCCCCGGCCGCCGGCCGCGCCCCGCGCCGGCGCGGGC-5'

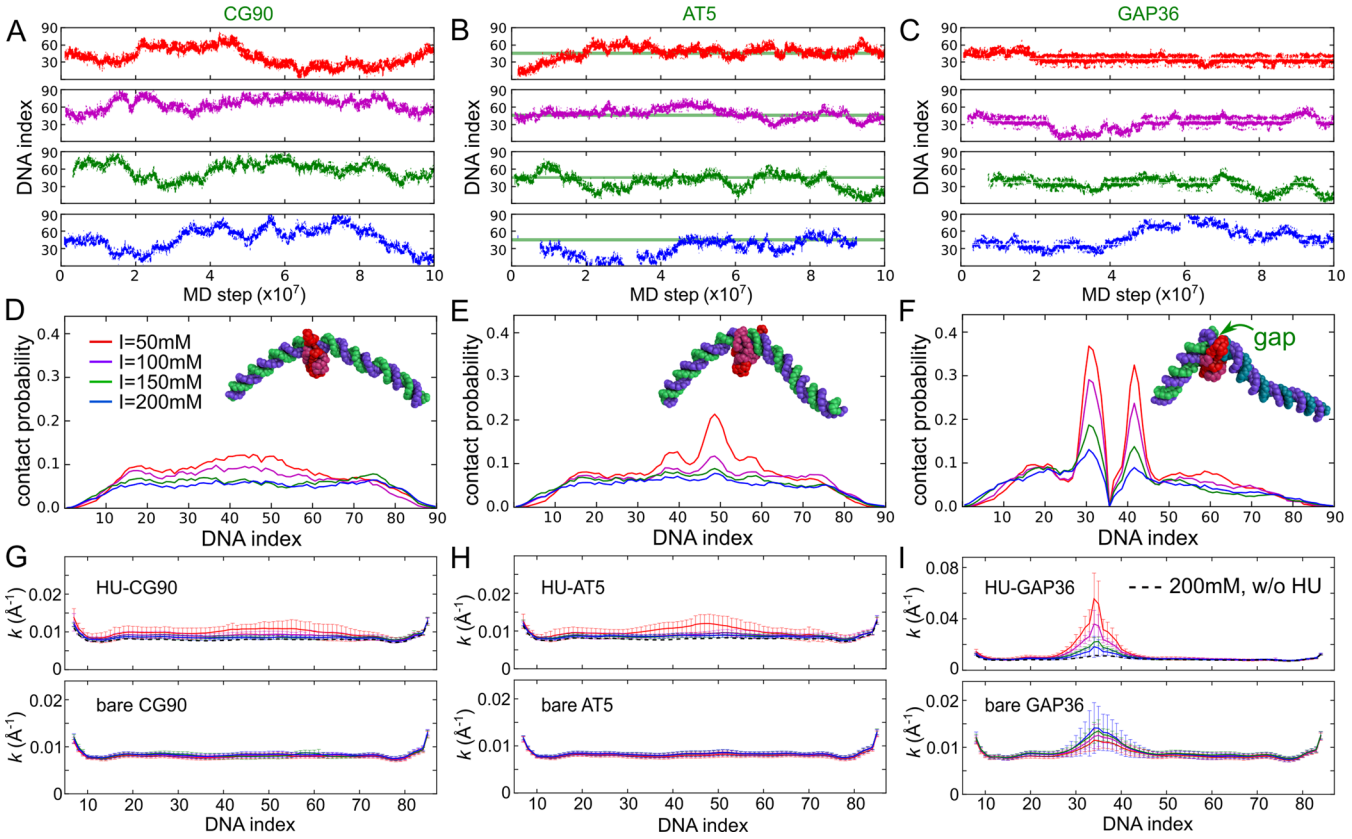

Figure 2. HU binding, HU sliding on DNA, and DNA curvature. (A–C) Time series of HU binding positions on DNA sequences CG90 (A), AT5 (B), and GAP36 (C), under ionic strengths of 50 mM (red), 100 mM (purple), 150 mM (green), and 200 mM (blue), respectively. (D–F) HU contact probability distribution of nucleotides from CG90 (D), AT5 (E), and GAP36 (F), with ionic strengths ranging from 50 mM to 200 mM. The insets show representative HU–DNA complex snapshots taken from I = 100 mM, when HU bound to the center of CG90 (D), or to the most probable binding positions on AT5 (E) and GAP36 (F). (G) Curvature of CG90 with (upper panel) and without (lower panel) the bound HU. Ionic strength color coding is the same as in (D). In the upper panel, the black dashed line shows the curvature of DNA without HU at 200 mM ionic strength. Panels (H) and (I) are the same as (G) but for AT5 and GAP36 sequences.

Figure 8C,D). We confirmed that the current model provides a good approximation of the experimental dissociation constant with the phosphate charge of $-1e$ (see Methods section and Figure 8D).

We then performed CG MD simulations for HU on five DNA sequences of 90 bp long: CG90, AT5, AT10, GAP36, and NICK36 (sequence feature are described below and shown in Figure 1C. Explicit sequences are in Table 1). For each DNA sequence, we repeated stochastic MD simulations of 10^8 MD steps 20 times at four monovalent salt concentrations of 50, 100, 150, and 200 mM. One MD step can roughly be mapped to 1 ps so that one trajectory corresponds to a 0.1 ms time scale.[70] In all the MD simulations, HU was initially placed at least 40 Å away from DNA. During the simulations, we monitored the binding/dissociation and sliding of HU on DNAs. Representative time courses of HU movements are plotted in Figure 2A for CG90, Figure 2B for AT5, and Figure 2C for GAP36. In each bound snapshot, plotted in the insets of Figure 2D–F, the HU protein typically contacts 7–15 bp.

For the case of CG90, a random sequence made of only C and G, HU quickly bound to and slid on the DNA, with rare dissociation events, at all salt concentrations studied. HU did not show any apparent preference for particular positions on DNA (Figure 2A). More quantitatively, when we plotted contact probabilities of HU on each nucleotide (Figure 2D), no significant pattern appeared except that HU disfavors the DNA

DOI: 10.1021/jacs.6b03729
J. Am. Chem. Soc. 2016, 138, 8512–8522

termini. Consistent with the dominant role of electrostatic interactions in HU−DNA binding, the increase in ionic strength weakens the attractive electrostatic interactions and thus results in lower HU contact probability to DNA.

The AT5 sequence contains 5 A/T base pairs at positions 46−50 with the rest of the sequence being the same as that of CG90. HU movements on the AT5 DNA were different from those on CG90 (Figure 2B). At 50 mM, after HU reached the A/T segment, it hovered around this region by the end of the simulations (Figure 2B, first panel). Statistical analysis of HU contact probabilities supports the conclusion that HU prefers the A/T-rich region at 50 mM ionic strength (Figure 2E, red line). Notably, in the contact probability distribution, other than the central major peak that corresponds to the A/T region, there are two lower shoulders, each located about 10 bp away from the central peak. These three peaks correspond to the nucleotides at the same orientation of the DNA duplex (Figure S1), and are thus spatially close to one another (Figure 2E inset). This suggests that HU can simultaneously bind to more than one of these sites, or bind to one site but can easily migrate from one to another. At ionic strengths higher than 50 mM, the HU binding preference for the A/T-rich region was weaker (Figure 2B), although small peaks can still be found in the HU contact probability distribution (Figure 2E). Similar results were also observed in our simulations of HU binding to AT10 (Figure S2A,C,E), whose sequence has 10 A/T base pairs at the center. These weak preferences for A/T sequences are consistent with the experiments mentioned above[60,61] and indicate that the CG models can accurately mimic the very subtle differences among heterogeneous DNA sequences and the precise characteristics of HU−DNA interactions.

In the simulations of HU binding to GAP36, which contains a gap at the 36th nucleotide with the rest of sequence being the same as that of CG90, we also monitored the HU binding positions to find out whether HU can recognize the gap. As can be seen in Figure 2C, at 50 mM ionic strength, after initial binding and relaxation, HU bound to the gap region (DNA index 25−45) and remained stationary at this region. Accordingly, the HU contact probability exhibits evident peaks around the gap region (Figure 2F). Notably, the peaks are much higher than those in the AT5 sequence. At higher ionic strengths, the time that HU stayed around the gap region is shorter than at 50 mM ionic strength (Figure 2C). Still, we see distinct peaks in the HU contact probability distributions at the same positions as seen in the 50 mM case (Figure 2F). This higher affinity of HU to the gap is also consistent with the experiments mentioned above.[62,63] At each ionic strength, a valley between two peaks in the contact probability distribution was observed at DNA index 36. Thus, HU does not prefer the gap itself, but prefer its neighbors. Combined with the representative structure (Figure 2F inset), we find that HU preferentially binds to nucleotides at the opposite side of the gap and then forms interactions that stabilize the bound conformation. More details on HU-GAP36 interactions will be discussed later in this paper. Similar results were found in the simulations of HU binding to NICK36 (DNA with a nick at index 36), for which the results are shown in Figure S2B,D,F.

By comparing the results of HU binding to CG90, AT5 (AT10), and GAP36 (NICK36), we showed that HU has weak preferences for the AT-rich region, but strongly favors binding to the near-gap/nick regions. These results are all in good agreement with the experiments.[60−63] Moreover, the experimental work classified HU as a structure-specific DNA-binding protein rather than a sequence-specific one.[62,71] Importantly, we observed significant DNA bending upon strong binding of HU (see below). The consistency of simulation results with experiments validates that the CG models and MD simulation methods used here are suitable for studying dynamic couplings between HU binding and DNA bending.

HU Binding Enhances DNA Bending. In our simulations, HU and DNA formed complex structures depicted in the insets of Figure 2D−F, in which DNAs are bent to different extents depending on their properties. To quantitatively evaluate the conformational changes of DNA upon HU binding, we monitored the local curvature of DNA (denoted as k) during the simulations (see Methods section and Figure S3A for details). The larger the value of k, the more sharply DNA bends. For comparison, we performed simulations for DNAs both with and without the bound HU.

In Figure 2G, we show the time-averaged curvature of CG90 as a function of DNA index, in the presence (upper panel) or absence (lower panel) of HU, respectively. For comparison, the curvature of naked DNA at 200 mM ionic strength is also shown in the upper panel (black dashed line). Upon HU binding the curvature of CG90 is slightly increased compared to the naked DNA, especially for the regions with higher HU contact probabilities. Similar results are also observed for AT5 (Figure 2H). We note that although the time-averaged effect of HU binding on DNA bending is not striking, at some certain snapshots, DNAs do have sharply bent conformations that are caused by interactions with HU, as in the inset of Figure 2E.

The effect of HU on the time-averaged curvature of the gapped DNA is much stronger than on CG90 and AT5. The curvatures of GAP36 with and without HU binding are shown in Figure 2I (note the difference in the scales of the vertical axes). As can be seen in the lower panel, the naked DNA exhibits spontaneous bending around the gap region at all ionic strengths. However, for HU-bound GAP36, we found that the binding of HU drastically enhanced the extent of DNA bending, especially at low ionic strength (Figure 2I upper panel). It can be seen that even at ionic strengths as high as 200 mM, which corresponds to weaker protein−DNA interactions, the bending of DNA bound with HU is much sharper than that of the bare DNA (Figure 2I). These results are consistent with the previous experimental observations in which HU binding enhances DNA bending.[61,64]

Notably, our results reveal that ionic strength has opposite effects on the curvature of GAP36 DNA with and without HU binding. For the naked DNA, where stiffness is dominated by the repulsive electrostatic interactions between the phosphate groups, the average curvature is smaller at lower ionic strength. At higher ionic strength, the average curvature is larger because of electrostatic screening (Figure 2I, lower panel). In contrast, the conformation of HU-bound DNA is largely dependent on the intermolecular electrostatic interactions between HU and DNA. Therefore, at lower ionic strength, stronger HU−DNA interactions engender a more sharply bent conformation of DNA than at higher ionic strength (Figure 2I upper panel). (Additional details below.) Similar results were also found for the bending of NICK36 (see Figure S3B).

DNA Bending Facilitates HU Binding. The above simulations showed that HU has a strong preference for a gap where DNA bends much more than the regular dsDNA. This preference can be attributed either to the chemical difference itself (lack of one nucleotide) or to its structural

DOI: 10.1021/jacs.6b03729
J. Am. Chem. Soc. 2016, 138, 8512−8522

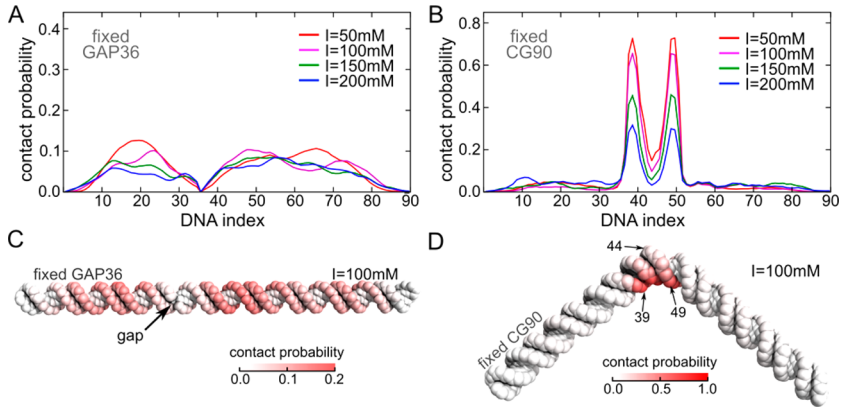

Figure 3. HU Binding to frozen DNAs. (A) HU contact probabilities to the GAP36 DNA frozen to the ideally straight B-type form at four different ionic strengths. (B) HU contact probabilities to the CG90 DNA frozen to the bent structure shown in (D). (C) The structure of the frozen GAP36 with each CG particle colored according to its HU contact probability at I = 100 mM. (D) The structure of the frozen CG90 that is bent at the center. Arrows mark the nucleotides at indexes 39, 44, and 49.

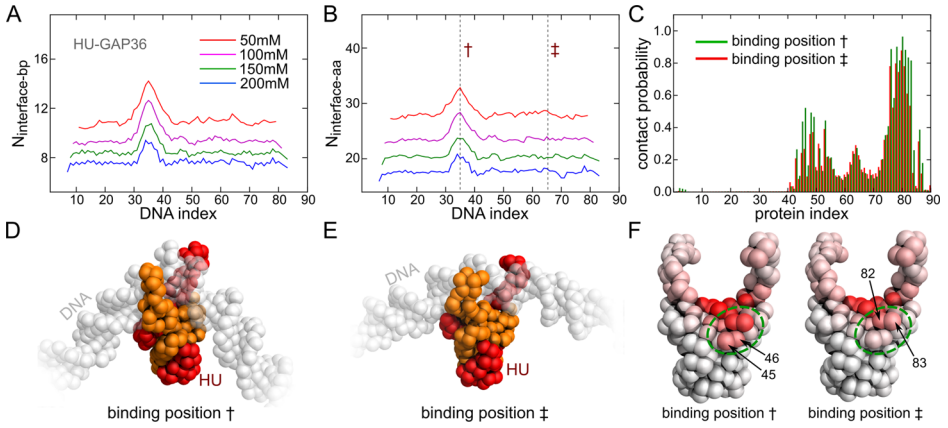

Figure 4. Two distinct modes of HU binding on GAP36. (A,B) Average number of base pairs (amino acid residues) that are in contact with HU (DNA) when HU binds to different positions along DNA. Colors of curves represent different ionic strengths. In (B), the two HU binding positions marked with † and ‡ are chosen for further analysis in (C)−(F). (C) DNA contact probabilities of HU residues, with HU binding to positions † (green) and ‡ (red). (D,E) Representative structures of the HU−DNA complexes when HU binds to positions † (D) and ‡ (E). The two subunits of HU are in orange and red, while DNAs are shown as transparent spheres for clarity. (F) Amino acids in HU are colored according to their DNA contact probabilities when HU binds to positions † (left) and ‡ (right). Residues that have large contact probability differences in two binding positions are labeled with their indices.

difference. To distinguish these two possibilities, we designed two control simulations in which DNA structures are frozen.

The first set employed the GAP36 DNA sequence frozen to the straight B-type DNA structure. HU lost its predilection for the near-gap region on this substrate; we plot the HU contact probabilities in Figure 3A,C. Combined with the HU binding probability for free GAP36 as shown in Figure 2F, these results clearly show that the propensity of HU for binding to the near-gap region cannot be explained by the difference in chemical moiety.

We next simulated HU binding to a CG90 DNA sequence frozen in a sharply bent structure (Figure 3D). This substrate lacks the chemical feature of GAP36 (the gap) but retains its salient structural feature (the sharp bend). We plot the HU contact probabilities in Figure 3B,D, where we find that HU strongly prefers binding to the sharply bent region. MD trajectories show that HU seldom left the bent region after binding to it (Figure S4). We observed two peaks and an in-between valley in the contact probabilities (Figure 3B), which is similar to the results of HU binding to GAP36 (Figure 2F). It is clear in Figure 3D that the two nucleotides with higher HU contact probabilities (indexes 39 and 49) are at the concave side of the DNA bend, while the nucleotide with low HU contact probability (index 44) is on the convex side. The negative charge density on the concave side is more prominent than on the convex side, so HU adopts interactions with nucleotides in the concave region. These results suggest that HUs binding specificity for DNA sequence or structure comes from its preference for the local bending of DNA.

Structural Insights into HU−DNA Interactions. We have shown that HU recognizes and induces changes in the local structure of DNA. We next sought structural insights into the HU−DNA binding interface.

First, we calculated the number of DNA base pairs and HU residues that are involved in HU−DNA binding interfaces when HU binds to and slides on CG90 and AT5 sequences. In each case, the number of contacts at the binding interface was nearly uniform across DNA-binding positions, excepting the terminal effects (Figure S5A−D). The number of contacts at the interface depended on the ionic strength: as the ionic strength increases from 50 to 200 mM, the average number of base pairs (for CG90 and AT5) in contact with HU, $N_{\text{interface-bp}}$,

DOI: 10.1021/jacs.6b03729
J. Am. Chem. Soc. 2016, 138, 8512−8522

decreases from ~11 to less than 8 (Figure S6A), and correspondingly, the average number of the interface amino acid residues, $N_{\text{interface-aa}}$, decreases from ~28 to ~18 (Figure S6B). Notably, the number of interface residues from our simulations approximates the experimental results (~9 bp) very well.[66]

Next, we performed a similar analysis for HU−DNA interface size in simulations of HU binding to the AT5 DNA frozen in the ideal straight form. We found that HU and DNA both contributed fewer interface residues when DNA was frozen than the case when DNA was not frozen (Figure S6A,B). This result clearly points to the "bendability" of DNA as an important factor for protein−DNA binding, as discussed above.

HU Binds to Linear and Gapped DNA Using Two Patterns. Continuing with the interface analysis, we show the number of base pairs ($N_{\text{interface-bp}}$) and amino acids ($N_{\text{interface-aa}}$) that exist in the binding interface of HU with GAP36 DNA sequence along the DNA index, in Figure 4A,B. When HU is bound to the gap region, $N_{\text{interface-bp}}$ is larger than when HU is bound to other regions by 2−4 bp (depending on ionic strength) (Figure 4A). Correspondingly, $N_{\text{interface-aa}}$ at the protein−DNA interface when HU is bound to the gap region is 4−6 larger than the case when HU is bound to other regions (Figure 4B).

We further analyzed the structures of HU−DNA complexes by focusing on two HU binding positions: DNA index 35 at the gap region (labeled † in Figure 4B) and DNA index 65 that is far from the gap (labeled ‡ in Figure 4B). Representative snapshots in each of the two positions are depicted in Figures 4D and E. We computed the DNA contact probability for each amino acid at the two HU binding positions (Figure 4C). Figure 4C shows that HU residues have higher probabilities of forming contacts with DNA when HU binds to position †, especially the amino acids around index 45−46 and those around index 82−83. We marked these residues (index 45, 46, 82, and 83) on the HU structures, where each CG residue is colored according to its DNA contact probability at positions † and ‡ (Figure 4F). The residues with distinct contact probabilities are spatially close to one another, and are on the "flanking" surface of HU (if we consider the β-arms as the "front side"). Based on these results, we conclude that DNA tends to form contacts with these flanking residues of HU, which consequently stabilize largely curved DNA, provided that the DNA is sufficiently bendable. When DNA wraps around HU and approaches the flanking residues, it is more sharply bent (Figure 4D); conversely, when DNA is less bent, it has a lower probability of contacting the flanking surfaces of HU (Figure 4E). These results provide new evidence for the dynamic relationship between the HU binding site size and the bending of DNA, which has also been proposed from the crystal structures of HU showing binding to DNA with altered structure.[59]

Polaron-like Sliding of HU. The results above show that HU binding and DNA bending are correlated in equilibrium-state probabilities. We next sought to address the dynamics of coupling. From MD trajectories of HU bound on the CG90 DNA, we found that highly curved DNA regions are largely overlapped with the binding positions of HU (Figure S7A), indicating that protein binding and DNA bending are dynamically coupled. In Figure 5A, the two-dimensional (2D) histogram demonstrated the correlation between HU binding site and the most bent position of DNA, based on statistics of 20 independent trajectories. As indicated by the most

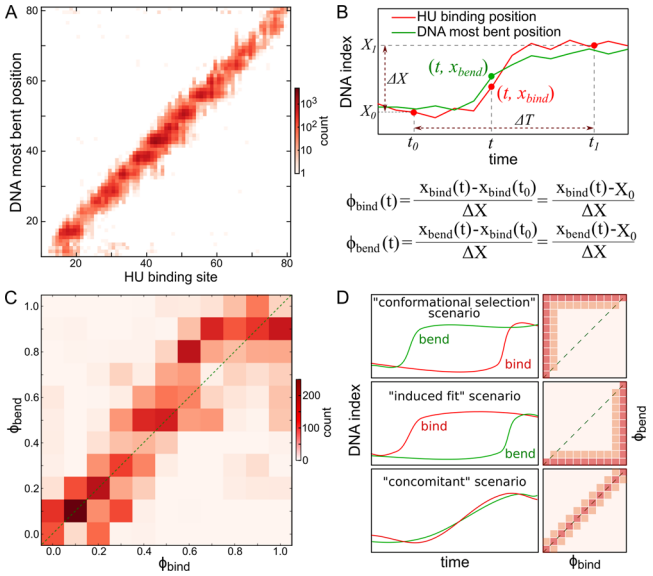

Figure 5. Dynamic coupling between HU binding and DNA bending. (A) 2D histogram of HU binding site versus the most bent position of DNA. Only the structures with the largest DNA curvature of $k \geq 0.04$ Å^{-1} were counted. The Pearson correlation coefficient between the two variables is 0.74. (B) Schematic plot of the coordinates we used in the analysis of short time scale correlation between HU sliding and spontaneous DNA bending. We monitored the HU binding position $x_{\text{bind}}(t)$ and the locally most bent DNA position $x_{\text{bend}}(t)$ during time interval ΔT. X_0 and X_1 are HU binding positions at time t_0 and t_1, and their difference is denoted as ΔX. Based on these quantities, we then defined two dimensionless coordinates, ϕ_{bind} and ϕ_{bend}, to describe HU sliding and dynamic DNA bending, respectively. (C) 2D histogram of ϕ_{bind} and ϕ_{bend} in short time scale transition events. A transition event is defined by $\Delta T = 1.0 \times 10^6$ and $\Delta X \geq 10$ bp. (D) Time series of x_{bend} (green curves) and x_{bind} (red curves) that can be classified into the "conformational selection", the "induced-fit", or the "concomitant" scenario of binding mechanism. Schematic 2D histograms of ϕ_{bind} and ϕ_{bend} for each case are shown on the right.

populated region on the diagonal (Figure 5A), HU binding and DNA bending are correlated throughout the long time scale trajectories, with the Pearson correlation coefficient of 0.74. In addition, one may observe nodal pattern in Figure 5A indicating some DNA regions are more highly bent than others. This inhomogeneity in flexibility is intrinsic property of the DNA sequence of CG90.

To further decipher the underlying mechanism of HU diffusion and its relation to DNA bending, we looked into shorter time scale dynamics. We picked out fragments of trajectories with the time length of $\Delta T = 10^6$ MD steps. If the displacement of HU in such a trajectory fragment is no less than 10 bp ($\Delta X \geq 10$ bp), it was defined as a "transition event". For each transition event, we then defined two dimensionless coordinates, ϕ_{bind} and ϕ_{bend}, to describe HU sliding and dynamic DNA bending, respectively (Figure 5B). During each time interval of ΔT, ϕ_{bind} changed from 0 to 1. DNA most bent position was highly coincident with HU binding position at the beginning and end of transitions, thus ϕ_{bend} changed from values ~0 (not necessarily = 0) to ~1 during ΔT. Additionally, statistical analysis of ϕ_{bind} and ϕ_{bend} can provide information on the underlying mechanism of binding coupled bending. As shown in the schematic plot Figure 5D, if the DNA most bent position spontaneously changes earlier than HU sliding (corresponding to $\phi_{\text{bend}} > \phi_{\text{bind}}$), this can be viewed as

DOI: 10.1021/jacs.6b03729
J. Am. Chem. Soc. 2016, 138, 8512−8522

"conformational selection". Conversely, if HU slides earlier than DNA bending changes (corresponding to $\phi_{bind} > \phi_{bend}$), the mechanism can be classified as "induced-fit". We plotted the 2D histogram of ϕ_{bind} and ϕ_{bend} in Figure 5C. From this plot, we can see that HU sliding and DNA bending moved concomitantly, which we cannot classify as historically long-standing "conformational selection" or "induced-fit" scenarios.

Conceptually, the DNA bending coupled HU sliding is similar to polaron. The polaron was originally defined as an electron that distorts neighboring phonons in condensed matters.[67,68] Due to their tight coupling, the electron and phonon distortions move together, like a quasi-particle. Later, cation migration on DNA was also treated as a polaron phenomenon.[72] In the current case, HU is highly positively charged and thus can be viewed as a multivalent cation.

DNA Curvature Regulates the Diffusion of HU. The results above show that HU binding is correlated with DNA bending, and sliding of HU is concomitant with DNA bending movement. We next sought to find out the effects of DNA curvature on HU sliding, like increased effective mass of electron in the case of polaron. As an example, we picked out a short fragment of the trajectory (2×10^6 steps) to demonstrate the sliding motions of HU. The time series of HU binding positions during this time interval is shown in Figure 6A (red dots and curve), together with the local DNA bending represented by blue intensity. At the beginning ($t < 3150 \times 10^4$) and ending ($t > 3250 \times 10^4$) of this time interval, DNA bent sharply at the HU binding site (dark blue areas), and HU sliding was localized within a narrow range. However, during the middle time range, $3150 < t < 3250$ ($\times 10^4$), DNA was less bent (light blue areas) and HU diffused in a wider range (Figure 6A). These results indicate that the HU movements are not simple diffusion, but are divided into pauses and transitions that occur intermittently and that the pauses and transitions correspond to high and low DNA curvature, respectively.

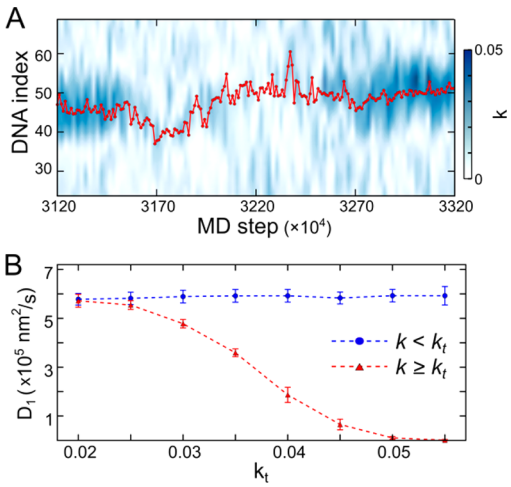

Figure 6. DNA bending regulated HU diffusion. (A) HU binding positions on CG90 (red dots) are highly coupled with the dynamic bending of DNA on a short time scale (2×10^6 steps). The DNA bending is represented by the blue color intensity as indicated by the bar on the right. (B) The diffusion coefficient of HU (D_1) as functions of DNA curvature at the HU binding site. With every value of DNA curvature (k_t), HU diffusion coefficients were calculated for $k < k_t$ and $k \geq k_t$ separately. Error bars indicate standard errors in the linear fit of D_1 from MSDs.

To quantitatively address the diffusion of HU on DNA and its dependence on DNA curvature, we calculated the one-dimensional diffusion coefficient D_1, defined by $D_1 = \mathrm{MSD}(\Delta t)/(2\Delta t)$, where $\mathrm{MSD}(\Delta t) = \langle (x_{bind}(t + \Delta t) - x_{bind}(t))^2 \rangle$ is the mean square displacement of the HU binding position as a function of time difference Δt. Figure 6B shows D_1 as functions of DNA curvature at the HU binding position (k_t). For each given k_t, we estimated HU sliding separately, when HU bound to less bent DNA ($k < k_t$) or when HU bound to sharper bent DNA ($k \geq k_t$). It is clear from Figure 6B that HU diffusion depends on different DNA curvatures. For DNA with a smaller curvature (blue dots), HU slides with a finite diffusion coefficient, whereas for larger DNA curvatures ($k \geq 0.05$ Å^{-1}), the effective diffusion coefficient is almost zero ($D_1 \approx 0$), which means the pause of HU sliding. More detailed statistical analysis of the HU diffusion motions also supports the conclusion that sharp DNA bending at HU binding positions results in HU pauses, and spontaneous relaxation of DNA bending allows intermittent HU diffusion (see Supporting Discussion and Figure S7). For a less bent DNA case, the estimated D_1 can approximately be mapped to 6×10^{-5} Å^2/step $\cong 6 \times 10^7$ Å^2/s, which is relatively large, but is within the range of measured diffusion coefficients for one-dimensional protein sliding along DNA.[27,28,73−75]

It is worth noting that previous analyses based on HU−DNA crystal structures and single-molecule experiments have revealed that the DNA bending in the HU−DNA complex is quite flexible, rather than fixed at a rigid angle.[59,64] In agreement with those data, here we show that HU-bound DNA can change between highly curved and less curved states, and the different bending states of DNA have significant effects on the binding mode and diffusion of HU. The ability of HU to stabilize varying curvatures of DNA enables the multifunctional roles that HU plays in many different cellular processes.

Investigation of 14 Other DNA-Binding Proteins. Finally, we address the generality of mutual dynamic coupling between protein binding to DNA and DNA bending, and polaron-like sliding. To this end, we performed MD simulations analogous to those performed with HU using 14 other DNA-binding protein domains. The protein domains studied cover all the major classes of DNA-binding protein domains, including the zinc-finger, the helix-turn-helix, the leucine-zipper coiled-coil, and the β-ribbon domain (protein names, PDB IDs, structures, and some properties are given in Figure S8). The substrate was a 100-bp pure C/G dsDNA excluding any specific sequence features.

By visually inspecting the binding positions of proteins and the curvatures of DNA (see Figure S9), we found varying degrees of coupling for the 14 proteins. Two proteins bent DNA much more than HU (the TATA box-binding protein (TBP) and the integration host factor (IHF), which is homologous to HU). At their binding sites, DNA was always highly bent. These also clearly exhibit polaron-like sliding. Three other proteins showed DNA curvatures similar to HU (SRF, serum response factor; GATA-1, the chicken erythroid transcription factor; and the VND homeodomain). In these cases, DNA was highly bent transiently, and less bent for the rest of time, which is very similar to the behavior of HU. The other 9 proteins showed less sharp DNA bending.

Of the three proteins that exhibited similar degrees of DNA bending to HU, here we report the results for the VND homeodomain as a representative. Figure 7A shows the 2D histogram of the VND-binding site and the most bent position

DOI: 10.1021/jacs.6b03729
J. Am. Chem. Soc. 2016, 138, 8512−8522

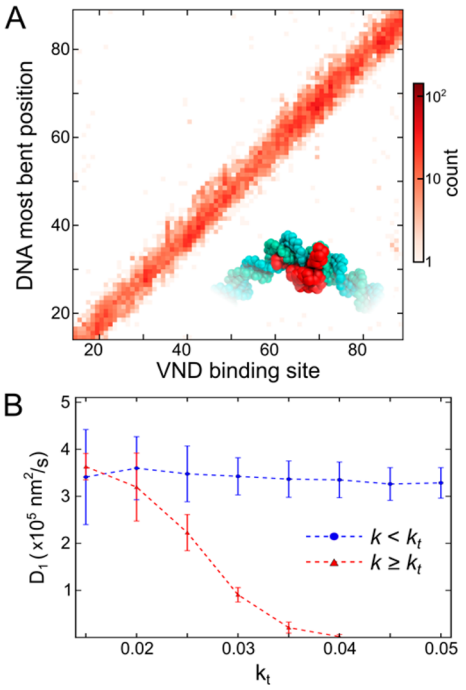

Figure 7. Protein binding to DNA, protein sliding, and DNA bending for the VND homeodomain. (A) 2D histogram of binding positions of the VND homeodomain (PDB ID: 1NK3) versus the most bent position of DNA. Only the structures with the largest DNA curvature of $k \geq 0.025$ Å^{-1} were counted. The Pearson correlation coefficient is 0.74. The inset shows representative simulated VND (red)−DNA (green) complex structure. (B) The diffusion coefficient of VND (D_1) as functions of DNA curvature at the VND-binding site. For every curvature value (k_t), diffusion coefficients of VND were calculated for $k < k_t$ and $k \geq k_t$ separately. Error bars indicate standard errors in the linear fit of D_1 from MSDs.

of DNA. As can be seen, DNA bending is highly coupled to VND binding, which is similar to the case of HU−DNA binding. Figure 7B plots the diffusion coefficients of VND when it binds to sharper bent DNA (red dots and curve) and less bent DNA (blue dots and curve). It is clear that when bound to sharper bent DNA, VND diffuses more slowly. With DNA curvature larger than 0.04 Å^{-1}, VND paused. We also show representative trajectories and structures of VND−DNA binding in Figure S10. Transient sharper/less DNA bending and the correspondingly slower/faster diffusion of VND were observed, as shown in Figure S10A−C. These results demonstrate the similarity between VND and HU in how they slide on DNA and the interplay between sliding and DNA bending. Since sequence-dependent deformations of the DNA has been shown to be important in the recognition by homeodomains,[12] the sliding motion regulated by the DNA curvature can be a mechanism which is the basis of accurate (sharp DNA bending allows slow exhaustive scanning) and efficient (less sharp DNA bending allows fast diffusion) search of its binding site.

CONCLUSION

In summary, we investigated the dynamic mechanism of sequence-nonspecific interactions between protein and DNA using HU as a model protein as well as 14 other proteins. The electrostatic interactions between positively charged protein residues and negatively charged DNA backbone groups modulated the binding and sliding behavior of HU as well as DNA bending. The HU−DNA binding interface was dynamically coupled to DNA curvature, and the number of contacts between HU and DNA determined the extent to which DNA bent. We found that HU motion on DNA has two distinct modes, sliding and pausing. In particular, HU paused when DNA was sharply bent. This type of complex interplay among protein binding, DNA bending, and protein sliding was a rather general mechanism in protein−DNA interactions; 6 out of 15 DNA-binding proteins examined here showed such couplings.

Some of our results can be thought as theoretical predictions which can be examined experimentally. For example, the current study suggests that the HU diffusion along DNA contains different modes; the fast diffusion mode and the pause mode. Once one can measure the distribution of position change in a fixed time interval, our study predicts that the distribution can be decomposed into two modes. Analysis of interface residues in HU revealed some flanking residues responsible for stabilizing the bent DNA. Mutations in these sites would alter the lifetime of the pause.

METHODS

Reference Structures. In the present work, we studied the binding of *E. coli* HUα_2 dimer to dsDNA. As the template structure of HU, we used the PDB entry 1MUL[76] for the dimerization core, and 1HUE[77] for the β-arms. The crystal structure 1MUL lacks the coordinates of the flexible β-arms (residues 58−71). These missing residues are modeled by using structural information from 1HUE. To make the model as accurate as possible, the "built-from-scratch" atomistic structure was refined through energy minimizations and molecular dynamics simulations with NAMD.[78]

The reference structures of all B-form dsDNAs were built with the 3DNA package.[79] As shown in Figure 1, we studied the binding of HU to one 35-bp DNA (S35) and several 90-bp DNAs (CG90, AT5, AT10, GAP36, and NICK36). The sequence of S35 was the same as that used in gel-mobility shift assays.[62] The sequence of CG90 was randomly chosen, and the sequences of AT5, AT10, GAP36, and NICK36 were prepared by introducing modifications to CG90. All the sequences are listed in Table 1.

To test the generality of our conclusion about the coupling among protein binding, sliding, and DNA bending, we simulated the binding of 14 other proteins to a 100-bp pure C/G DNA sequence. The reference structures of proteins were taken from their corresponding PDB files (see Figure S8 for a full list).

Protein Modeling. To model the interactions between amino acid residues, we employed the AICG2+ potentials[45] coupled to the Debye−Hückel-type electrostatic interaction. The AICG2+ energy function is given by $V_{pro} = V_{local} + V_{G\bar{o}} + V_{exv}$. Details of the local potentials (V_{local}), the G$\bar{o}$-type potentials for native contacts ($V_{G\bar{o}}$), and the excluded volume potentials for non-native interactions (V_{exv}) are described in the Supporting Information. For the flexible regions in HU (residues 55, 56, 72, and 73), which connect the β-arms and the dimerization core, G$\bar{o}$-type interactions with other parts were removed. G$\bar{o}$-type interactions between the β-arms and the dimerization core were also turned off to keep their motions independent. A similar protein model was applied to all the other proteins we studied.

DNA Model. In the present work, we used the 3SPN.2C model developed by de Pablo's group to model dsDNA.[46,80] In this model each nucleotide is represented by three CG particles corresponding to the phosphate group (P), sugar (S), and base (B). The interactions among these particles include structure-based local potentials, base-pairing, intrastrand base-stacking, interstrand cross-stacking, excluded volume effects, and Debye−Hückel-type electrostatic interactions.[80] Note that to take into account of the local counterion condensation effect,[81] the charge of phosphate in the 3SPN.2C model is $q_P = -0.6e$. This model has been tuned to reproduce geometric, mechanical, and

DOI: 10.1021/jacs.6b03729
J. Am. Chem. Soc. 2016, 138, 8512−8522

thermodynamic properties of dsDNA. The sequence-dependent shape and flexibility are also incorporated,[46] which is important in protein−DNA interactions. Especially, the bonded and nonbonded energy parameters as well as the reference structure are carefully tuned to accurately represent DNA shape properties such as sequence-dependent minor groove width.[46,82]

Protein−DNA Interactions. For protein−DNA interactions, we included the excluded volume effect and the electrostatic interactions. For the former, we used residue-type-dependent radii for both amino acids and nucleotides (see Supporting Information). The latter was modeled using the Debye−Hückel theory.

Since the electrostatic interaction is the dominant factor in protein−DNA interactions, we paid special attention to this term in the study of protein−DNA binding. As for proteins, we employed the RESPAC method[83] to determine the partial charges of the CG beads that give the best approximation of the electrostatic potential calculated from the all-atom models. The results of RESPAC for HU are shown in Figure 8A,B.

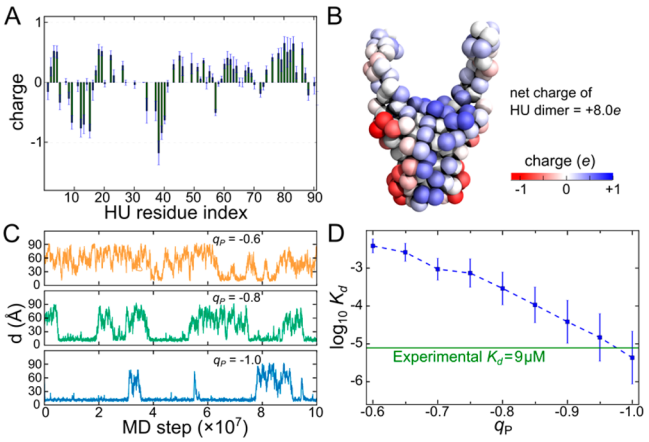

Figure 8. Binding of HU to 35-bp dsDNA (S35). (A) The charges of coarse-grained HU residues calculated using the RESPAC method. (B) The charge distribution of HU residues. The CG particles are colored according to their charge values, as indicated by the color bar. (C) Time series of distance from the center of mass of HU to the surface of DNA (d), with different values of phosphate charge (q_P). (D) Simulated dissociation constant (K_d) as a function of q_P. The green line shows the experimental result of K_d = 9 μM.

As described above, the phosphate charge in the 3SPN.2C model is set to −0.6e to account for the counterion condensation effect within dsDNA.[80] However, most interactions between protein and DNA are attractive and considered as short-range direct contacts. Thus, the counterion effect must be weakened in protein−DNA interactions. In the present work, we calibrated the charge of phosphate for protein−DNA short-range interactions and determined the optimal value of q_P that reproduces the dissociation constant (K_d) from experiments[62] (Figure 8C,D). We found that the phosphate charge value of q_P = −1.0e is the best choice and was used for subsequent protein−DNA interactions in the product simulations. Note that we still used the phosphate charge value of q_P = −0.6e within dsDNA.

Molecular Dynamics Simulations. All the CG simulations were performed by the CafeMol package.[84] The simulations were conducted by Langevin dynamics with a friction coefficient γ = 0.02 at temperature T = 298 K.

In the simulations to calibrate q_P, the distance between the center-of-mass (COM) of HU and S35 DNA were constrained to be smaller than 100 Å, which sets the effective concentration. Nine q_P values ranging from −0.6 to −1.0e were tested at the ionic strength of 200 mM. For each charge value, 20 independent 10^8-step simulations were performed. The first 10^7 frames in each trajectory were neglected in the posterior analysis.

In the production runs, the COM distance between HU and 90-bp DNA was constrained to be smaller than 300 Å. The ionic strength was set to 50, 100, 150, and 200 mM, and for each ionic strength, 20 simulations were carried out independently, each for 10^8 steps. In the statistics of contact probability and geometric properties (described below), structures from the first 2 × 10^7 frames were discarded.

Analysis. In any contact analysis, we defined that a pair of CG particles is in contact when their distance is less than 7 Å. For the ensemble in which HU is bound to DNA, the conditional DNA contact probability of the ith residue in HU (plotted in Figure 4C) was defined by

$$P_i(\tau) = \frac{\sum_\tau \delta_i(\tau)}{\sum_\tau \Delta(\tau)}$$

Here, τ is simulation time; $\delta_i(\tau)$ = 1 if the ith HU residue forms a contact with any CG particle from DNA at time τ, $\delta_i(\tau)$ = 0, otherwise; $\Delta(\tau)$ = 1 if any HU particle forms a contact with DNA, $\Delta(\tau)$ = 0 otherwise. The HU contact probability of ith bp of DNA was defined the same way. Here, when any particle in a bp (containing 6 particles) is in contact with HU, we set $\delta_i(\tau)$ = 1.

For the HU−DNA binding interface, we computed the number of residues in HU (N_{aa}) and the number of base pairs in DNA (N_{bp}) that form intermolecular contacts with each other to estimate the interface size at time τ:

$$N_{\text{interface-aa}}(\tau) = \sum_{i\in\text{HU}} \delta_i(\tau)$$

$$N_{\text{interface-bp}}(\tau) = \sum_{i\in\text{DNA}} \delta_i(\tau)$$

Here $\delta_i(\tau)$ has the same definition as described above.

In the discussions of HU binding coupled to DNA bending and HU−DNA interface size, we need a single-value expression of HU binding position. To describe the binding position, we used the mean DNA index of the nucleotides that are in contact with HU:

$$x_{\text{bind}}(\tau) = \frac{\sum_{i\in\text{DNA}} i\delta_i(\tau)}{N_{\text{interface-bp}}(\tau)}$$

To quantitatively evaluate the bending extent of DNA, we used the curvature of the double helix (Figure S3A). Calculation of the curvature as well as the major/minor groove widths were carried out using homemade scripts based on algorithms proposed by Stofer et al.[85]

The structural graphics were plotted using the PyMOL package.[86]

■ ASSOCIATED CONTENT

Supporting Information

The Supporting Information is available free of charge on the ACS Publications website at DOI: 10.1021/jacs.6b03729.

Additional descriptions of the simulation methods and data analysis; supporting discussions; Table S1; Figures S1−S11 (PDF)

■ AUTHOR INFORMATION

Corresponding Author

*takada@biophys.kyoto-u.ac.jp

Notes

The authors declare no competing financial interest.

■ ACKNOWLEDGMENTS

This work was supported in part by the MEXT KAKENHI 15H01351, 26104517, and 25251019, and in part by the Strategic Programs for Innovative Research "Supercomputational Life Science" of MEXT. We thank Daniel Duzdevich for helpful English editing.

DOI: 10.1021/jacs.6b03729
J. Am. Chem. Soc. 2016, 138, 8512−8522

REFERENCES

(1) Kalodimos, C. G. *Science* **2004**, *305* (5682), 386.
(2) Halford, S. E. *Nucleic Acids Res.* **2004**, *32* (10), 3040.
(3) Esadze, A.; Kemme, C. A.; Kolomeisky, A. B.; Iwahara, J. *Nucleic Acids Res.* **2014**, *42* (11), 7039.
(4) Dillon, S. C.; Dorman, C. J. *Nat. Rev. Microbiol.* **2010**, *8* (3), 185.
(5) Brackley, C. A.; Taylor, S.; Papantonis, A.; Cook, P. R.; Marenduzzo, D. *Proc. Natl. Acad. Sci. U. S. A.* **2013**, *110* (38), E3605.
(6) Thompson, J. F.; Landy, A. *Nucleic Acids Res.* **1988**, *16* (20), 9687.
(7) Paull, T. T.; Haykinson, M. J.; Johnson, R. C. *Genes Dev.* **1993**, *7* (8), 1521.
(8) Masse, J. E.; Wong, B.; Yen, Y.-M.; Allain, F. H.-T.; Johnson, R. C.; Feigon, J. *J. Mol. Biol.* **2002**, *323* (2), 263.
(9) Stella, S.; Cascio, D.; Johnson, R. C. *Genes Dev.* **2010**, *24* (8), 814.
(10) Bhattacherjee, A.; Levy, Y. *Nucleic Acids Res.* **2014**, *42* (20), 12404.
(11) Bhattacherjee, A.; Levy, Y. *Nucleic Acids Res.* **2014**, *42* (20), 12415.
(12) Rohs, R.; West, S. M.; Sosinsky, A.; Liu, P.; Mann, R. S.; Honig, B. *Nature* **2009**, *461* (7268), 1248.
(13) Rohs, R.; West, S. M.; Liu, P.; Honig, B. *Curr. Opin. Struct. Biol.* **2009**, *19* (2), 171.
(14) Bellomy, G. R.; Mossing, M. C.; Record, M. T. *Biochemistry* **1988**, *27* (11), 3900.
(15) Liu-Johnson, H.-N.; Gartenberg, M. R.; Crothers, D. M. *Cell* **1986**, *47* (6), 995.
(16) Czapla, L.; Peters, J. P.; Rueter, E. M.; Olson, W. K.; Maher, L. J. *J. Mol. Biol.* **2011**, *409* (2), 278.
(17) Richmond, T. J.; Luger, K.; Mäder, A. W.; Richmond, R. K.; Sargent, D. F. *Nature* **1997**, *389* (6648), 251.
(18) Thanbichler, M.; Wang, S. C.; Shapiro, L. *J. Cell. Biochem.* **2005**, *96* (3), 506.
(19) Miele, V.; Vaillant, C.; D'Aubenton-Carafa, Y.; Thermes, C.; Grange, T. *Nucleic Acids Res.* **2008**, *36* (11), 3746.
(20) Parvin, J. D.; McCormick, R. J.; Sharp, P. A.; Fisher, D. E. *Nature* **1995**, *373* (6516), 724.
(21) Vivas, P.; Velmurugu, Y.; Kuznetsov, S. V.; Rice, P. A.; Ansari, A. *J. Mol. Biol.* **2012**, *418* (5), 300.
(22) Becker, N. A.; Maher, L. J. *Proc. Natl. Acad. Sci. U. S. A.* **2015**, *112* (23), 7177.
(23) Joshi, R.; Passner, J. M.; Rohs, R.; Jain, R.; Sosinsky, A.; Crickmore, M. A.; Jacob, V.; Aggarwal, A. K.; Honig, B.; Mann, R. S. *Cell* **2007**, *131* (3), 530.
(24) Wang, H.; Yang, Y.; Schofield, M. J.; Du, C.; Fridman, Y.; Lee, S. D.; Larson, E. D.; Drummond, J. T.; Alani, E.; Hsieh, P.; Erie, D. a. *Proc. Natl. Acad. Sci. U. S. A.* **2003**, *100* (25), 14822.
(25) Negureanu, L.; Salsbury, F. R. *J. Biomol. Struct. Dyn.* **2014**, *32* (6), 969.
(26) Salsbury, F. R.; Clodfelter, J. E.; Gentry, M. B.; Hollis, T.; Scarpinato, K. D. *Nucleic Acids Res.* **2006**, *34* (8), 2173.
(27) Murata, A.; Ito, Y.; Kashima, R.; Kanbayashi, S.; Nanatani, K.; Igarashi, C.; Okumura, M.; Inaba, K.; Tokino, T.; Takahashi, S.; Kamagata, K. *J. Mol. Biol.* **2015**, *427* (16), 2663.
(28) Wang, Y. M.; Austin, R. H.; Cox, E. C. *Phys. Rev. Lett.* **2006**, *97* (4), 048302.
(29) Yao, N. Y.; Georgescu, R. E.; Finkelstein, J.; O'Donnell, M. E. *Proc. Natl. Acad. Sci. U. S. A.* **2009**, *106* (32), 13236.
(30) Kad, N. M.; Wang, H.; Kennedy, G. G.; Warshaw, D. M.; Van Houten, B. *Mol. Cell* **2010**, *37* (5), 702.
(31) Townson, S. A.; Samuelson, J. C.; Bao, Y.; Xu, S.; Aggarwal, A. K. *Structure* **2007**, *15* (4), 449.
(32) Nelson, S. R.; Dunn, A. R.; Kathe, S. D.; Warshaw, D. M.; Wallace, S. S. *Proc. Natl. Acad. Sci. U. S. A.* **2014**, *111* (20), E2091.
(33) Terakawa, T.; Kenzaki, H.; Takada, S. *J. Am. Chem. Soc.* **2012**, *134* (35), 14555.
(34) Vuzman, D.; Levy, Y. *Mol. BioSyst.* **2012**, *8* (1), 47.
(35) Marcovitz, A.; Levy, Y. *Proc. Natl. Acad. Sci. U. S. A.* **2011**, *108* (44), 17957.
(36) Givaty, O.; Levy, Y. *J. Mol. Biol.* **2009**, *385* (4), 1087.
(37) Villa, E.; Balaeff, A.; Schulten, K. *Proc. Natl. Acad. Sci. U. S. A.* **2005**, *102* (19), 6783.
(38) Pan, Y.; Nussinov, R. *J. Biol. Chem.* **2007**, *282* (1), 691.
(39) Kenzaki, H.; Takada, S. *PLoS Comput. Biol.* **2015**, *11* (8), e1004443.
(40) Silva, D.-A.; Weiss, D. R.; Pardo Avila, F.; Da, L.-T.; Levitt, M.; Wang, D.; Huang, X. *Proc. Natl. Acad. Sci. U. S. A.* **2014**, *111* (21), 7665.
(41) Vuzman, D.; Azia, A.; Levy, Y. *J. Mol. Biol.* **2010**, *396* (3), 674.
(42) Sim, A. Y.; Minary, P.; Levitt, M. *Curr. Opin. Struct. Biol.* **2012**, *22* (3), 273.
(43) Potoyan, D. A.; Savelyev, A.; Papoian, G. A. *Wiley Interdiscip. Rev. Comput. Mol. Sci.* **2013**, *3* (1), 69.
(44) Chen, J.; Darst, S. A.; Thirumalai, D. *Proc. Natl. Acad. Sci. U. S. A.* **2010**, *107* (28), 12523.
(45) Li, W.; Wang, W.; Takada, S. *Proc. Natl. Acad. Sci. U. S. A.* **2014**, *111* (29), 10550.
(46) Freeman, G. S.; Hinckley, D. M.; Lequieu, J. P.; Whitmer, J. K.; de Pablo, J. J. *J. Chem. Phys.* **2014**, *141* (16), 165103.
(47) Freeman, G. S.; Lequieu, J. P.; Hinckley, D. M.; Whitmer, J. K.; de Pablo, J. J. *Phys. Rev. Lett.* **2014**, *113* (16), 168101.
(48) Potoyan, D. A.; Zheng, W.; Komives, E. A.; Wolynes, P. G. *Proc. Natl. Acad. Sci. U. S. A.* **2016**, *113* (1), 110.
(49) Rouvière-Yaniv, J.; Yaniv, M.; Germond, J.-E. *Cell* **1979**, *17* (2), 265.
(50) Lia, G.; Bensimon, D.; Croquette, V.; Allemand, J.-F.; Dunlap, D.; Lewis, D. E. A.; Adhya, S.; Finzi, L. *Proc. Natl. Acad. Sci. U. S. A.* **2003**, *100* (20), 11373.
(51) Lewis, D. E. A.; Geanacopoulos, M.; Adhya, S. *Mol. Microbiol.* **1999**, *31* (2), 451.
(52) Hashimoto, M.; Imhoff, B.; Ali, M. M.; Kow, Y. W. *J. Biol. Chem.* **2003**, *278* (31), 28501.
(53) Kow, Y. W.; Imhoff, B.; Weiss, B.; Hung, D. C. I.; Hindoyan, A. A.; Story, R. M.; Goodman, S. D. *Nucleic Acids Res.* **2007**, *35* (19), 6672.
(54) Kamashev, D.; Rouviere-Yaniv, J. *EMBO J.* **2000**, *19* (23), 6527.
(55) Swinger, K. K.; Rice, P. A. *Curr. Opin. Struct. Biol.* **2004**, *14* (1), 28.
(56) Claret, L.; Rouviere-Yaniv, J. *J. Mol. Biol.* **1997**, *273* (1), 93.
(57) Guo, F.; Adhya, S. *Proc. Natl. Acad. Sci. U. S. A.* **2007**, *104* (11), 4309.
(58) Kannan, A.; Camilloni, C.; Sahakyan, A. B.; Cavalli, A.; Vendruscolo, M. *J. Am. Chem. Soc.* **2014**, *136* (6), 2204.
(59) Swinger, K. K. *EMBO J.* **2003**, *22* (14), 3749.
(60) Prieto, A. I.; Kahramanoglou, C.; Ali, R. M.; Fraser, G. M.; Seshasayee, A. S. N.; Luscombe, N. M. *Nucleic Acids Res.* **2012**, *40* (8), 3524.
(61) Swinger, K. K.; Rice, P. A. *J. Mol. Biol.* **2007**, *365* (4), 1005.
(62) Pinson, V.; Takahashi, M.; Rouviere-Yaniv, J. *J. Mol. Biol.* **1999**, *287* (3), 485.
(63) Zelwer, C. *J. Biol. Chem.* **1995**, *270* (17), 10291.
(64) van Noort, J.; Verbrugge, S.; Goosen, N.; Dekker, C.; Dame, R. T. *Proc. Natl. Acad. Sci. U. S. A.* **2004**, *101* (18), 6969.
(65) Koh, J.; Saecker, R. M.; Record, M. T. *J. Mol. Biol.* **2008**, *383* (2), 324.
(66) Bonnefoy, E.; Rouvière-Yaniv, J. *EMBO J.* **1991**, *10* (3), 687.
(67) Landau, L. D. *Phys. Z. Sowjetunion* **1933**, *3*, 644.
(68) Landau, L. D.; Pekar, S. I. In *Collected Papers of L.D. Landau*; Elsevier, 1965; Vol. *53*, pp 478−483.
(69) Fleming, G. R.; Wolynes, P. G. *Phys. Today* **1990**, *43* (5), 36.
(70) Takada, S.; Kanada, R.; Tan, C.; Terakawa, T.; Li, W.; Kenzaki, H. *Acc. Chem. Res.* **2015**, *48* (12), 3026.
(71) Wojtuszewski, K.; Mukerji, I. *Biochemistry* **2003**, *42* (10), 3096.
(72) Henderson, P. T.; Jones, D.; Hampikian, G.; Kan, Y.; Schuster, G. B. *Proc. Natl. Acad. Sci. U. S. A.* **1999**, *96* (15), 8353.
(73) Gorman, J.; Greene, E. C. *Nat. Struct. Mol. Biol.* **2008**, *15* (8), 768.

DOI: 10.1021/jacs.6b03729
J. Am. Chem. Soc. 2016, 138, 8512−8522

(74) Tafvizi, A.; Huang, F.; Leith, J. S.; Fersht, A. R.; Mirny, L. a; van Oijen, A. M. *Biophys. J.* **2008**, *95* (1), L01.
(75) Blainey, P. C.; Luo, G.; Kou, S. C.; Mangel, W. F.; Verdine, G. L.; Bagchi, B.; Xie, X. S. *Nat. Struct. Mol. Biol.* **2009**, *16* (12), 1224.
(76) Ramstein, J.; Hervouet, N.; Coste, F.; Zelwer, C.; Oberto, J.; Castaing, B. *J. Mol. Biol.* **2003**, *331* (1), 101.
(77) Vis, H.; Mariani, M.; Vorgias, C. E.; Wilson, K. S.; Kaptein, R.; Boelens, R. *J. Mol. Biol.* **1995**, *254* (4), 692.
(78) Phillips, J. C.; Braun, R.; Wang, W.; Gumbart, J.; Tajkhorshid, E.; Villa, E.; Chipot, C.; Skeel, R. D.; Kalé, L.; Schulten, K. *J. Comput. Chem.* **2005**, *26* (16), 1781.
(79) Lu, X.-J.; Olson, W. K. *Nat. Protoc.* **2008**, *3* (7), 1213.
(80) Hinckley, D. M.; Freeman, G. S.; Whitmer, J. K.; de Pablo, J. J. *J. Chem. Phys.* **2013**, *139* (14), 144903.
(81) Hayes, R. L.; Noel, J. K.; Mandic, A.; Whitford, P. C.; Sanbonmatsu, K. Y.; Mohanty, U.; Onuchic, J. N. *Phys. Rev. Lett.* **2015**, *114* (25), 258105.
(82) Lu, X.-J.; Olson, W. K. *Nucleic Acids Res.* **2003**, *31* (17), 5108.
(83) Terakawa, T.; Takada, S. *J. Chem. Theory Comput.* **2014**, *10* (2), 711.
(84) Kenzaki, H.; Koga, N.; Hori, N.; Kanada, R.; Li, W.; Okazaki, K.; Yao, X.-Q.; Takada, S. *J. Chem. Theory Comput.* **2011**, *7* (6), 1979.
(85) Stofer, E.; Lavery, R. *Biopolymers* **1994**, *34* (3), 337.
(86) *PyMOL*; Schrodinger LLC, 2015.

DOI: 10.1021/jacs.6b03729
J. Am. Chem. Soc. 2016, 138, 8512−8522